sustainability

MDPI

Article

Application of Catalytic H_2O_2-Mediated NOx Removal Process Leveraging Solid Waste Residues: Exemplified by Copper Slag

Huidong Tang [1], Jiacheng Bao [2], Chen Liu [1], Yuwen Deng [1], Yixing Ma [1], Lei Shi [1], Shuangyou Bao [1,*], Kai Li [1], Ping Ning [1] and Xin Sun [1,*]

[1] Faculty of Environmental Science and Engineering, Kunming University of Science and Technology, Kunming 650500, China; tanghuidong2025@163.com (H.T.); liuchen_2021@126.com (C.L.); yuwen_ddd@163.com (Y.D.); mayixing99@kust.edu.cn (Y.M.); ahdyshilei@163.com (L.S.); likaichi@163.com (K.L.); ningpingkmust@163.com (P.N.)

[2] School of Resource & Environment and Safety Engineering, University of South China, Hengyang 421001, China; jcbao@usc.edu.cn

* Correspondence: baoshuangyou@163.com (S.B.); sunxin_kmust@163.com (X.S.)

Abstract: In pursuing sustainable environmental solutions, the concept of 'waste to treasure' has emerged as a promising approach. In this study, a new process is proposed to combine solid copper slag with hydrogen peroxide (H_2O_2) to remove nitrogen oxides (NOx) from acidic exhaust gases, thus effectively utilizing waste materials. Firstly, different smelting slags were screened to determine the catalytic potential of copper slag for hydrogen peroxide. Subsequently, the catalytic activity of the copper slags at various stages of the copper smelting process was thoroughly evaluated and optimized. In addition, a multifactorial evaluation of slow-cooled copper slag catalysts for removing NOx was carried out. Preliminary indications are that the iron phase in the copper slag is identified as the main source of catalytic activity sites. The results suggest that Fe^{2+}/Fe^{3+} sites on the surface of the Fe phase in the slow-cooled copper slag may be crucial in improving the NOx removal efficiency. The main reactive oxygen species detected in the system were ·OH, $\cdot O_2^-$, and $^1O_2$. In addition, the transformation products, formation pathways, and reaction mechanisms of NO in the liquid phase were initially investigated and determined. This study provides a green and sustainable path for the utilization of solid waste and management of atmospheric fumes in the non-ferrous metal industry and offers new perspectives to address environmental challenges in industrial processes.

Keywords: copper slag; hydrogen peroxide; denitrification; solid waste utilization; screening optimization

check for updates

Academic Editor: Chao Gai

Received: 7 February 2025
Revised: 4 March 2025
Accepted: 10 March 2025
Published: 11 March 2025

Citation: Tang, H.; Bao, J.; Liu, C.; Deng, Y.; Ma, Y.; Shi, L.; Bao, S.; Li, K.; Ning, P.; Sun, X. Application of Catalytic H_2O_2-Mediated NOx Removal Process Leveraging Solid Waste Residues: Exemplified by Copper Slag. *Sustainability* **2025**, *17*, 2469. https://doi.org10.3390/su17062469

Copyright: © 2025 by the authors. Licensee MDPI, Basel, Switzerland. This article is an open access article distributed under the terms and conditions of the Creative Commons Attribution (CC BY) license (https://creativecommons.org/licenses/by/4.0/).

1. Introduction

In the realm of industrial processes, especially within the non-ferrous metal smelting industry, the emission of nitrogen oxides (NOx) has become a paramount environmental concern [1,2]. Once released into the atmosphere, NOx of reactive contaminants can cause a range of serious environmental problems due to poor prediction and management of their fate and transport [3]. Acid rain, formed when NOx reacts with water vapor and other substances in the air, can corrode buildings, ravage forests, and acidify water bodies, thereby disrupting the ecological balance of aquatic ecosystems [4,5]. Photochemical smog, another consequence of NOx emissions, is a complex cocktail of pollutants that can trigger respiratory problems, cause eye irritation, and bring about other health issues for humans. Furthermore, NOx significantly contributes to the formation of haze, diminishing visibility and degrading air quality in urban and industrial areas [4–7].

Traditional techniques for curbing NOx emissions from industrial flue gas, such as selective catalytic reduction (SCR) and selective non-catalytic reduction (SNCR), have been extensively applied [4,8]. Nevertheless, these methods come with several inherent drawbacks. SCR necessitates the use of expensive catalysts, like vanadium-based catalysts [9]. These catalysts are not only costly but also have a finite lifespan and can cause environmental pollution when they are discarded. SNCR, on the other hand, typically demands high-temperature operating conditions, resulting in high energy consumption. Additionally, both methods may generate secondary pollutants. For example, SCR may also lead to ammonia leakage, which can confuse the environmental management of industrial emissions [4,9]. Therefore, compared with the dry reduction method for the denitrification of nitrogen oxides, slurry wet flue gas denitrification (NOx removal) can effectively avoid the problem of catalyst poisoning due to the complexity of the flue gas type and the reduction in safety accidents caused by ammonia leakage.

In recent years, the concept of "waste for waste" has gained significant attention in the environmental protection field [10,11]. This approach focuses on the innovative use of solid waste materials to solve ecological problems, presenting a sustainable solution that combines waste reduction with environmental improvement [12–14]. Currently, Bao et al. [15] have made progress in simultaneous flue gas desulfurization and denitrification using copper slag solid waste combined with potassium permanganate, achieving denitrification efficiencies as high as 84.4%. Meanwhile, Tang et al. [16] have used manganese slag solid waste to modify iron-manganese synergistically, catalyzing PMS thermally and investigating the performance of organic matter degradation in water treatment. Yang et al. [17] investigated reaction kinetics and the desulfurization performance of desulfurization of lead and zinc slag. Su et al. [18] investigated the properties of gel materials prepared from slag/fly ash. Although there exists a large amount of nonferrous metal waste at the back-end of nonferrous metal smelting, such as lead–zinc slag [19], manganese slag [16], and copper slag [20], there is still a lack of more effective utilization methods. Taking copper smelting as an example, copper slag is a by-product of the copper smelting process, which exists in large quantities worldwide. Most of this copper slag is disposed of in landfills, which not only occupies precious land resources but also poses a risk of soil and groundwater contamination due to the leaching of heavy metals and other harmful substances [21,22]. However, copper slag contains a variety of metal oxides and minerals that can confer unique catalytic properties to the slag. Therefore, we conducted a study combining solid waste feedstock with hydrogen peroxide, which not only avoids the secondary water pollution caused by the use of potassium permanganate, as mentioned above, but also improves the data on the application of catalytic removal of nitrogen oxides from waste residues such as copper slag.

Hydrogen peroxide (H_2O_2), a green and eco-friendly oxidant, has been increasingly used in environmental applications. Under appropriate conditions, it decomposes into water and oxygen, leaving no harmful residues [6,23]. The combination of copper slag and hydrogen peroxide for the removal of NOx from acid tail gas represents a novel and promising approach. This method has the following advantages: it improves the high-value utilization of solid waste, reduces the cost of the catalyst used, and mitigates the secondary pollution of the oxidant. It not only provides an effective way to recycle copper slag, a solid waste material, but also offers a more sustainable and efficient solution for NOx control in the non-ferrous metal smelting industry [24].

The primary objective of this study was to explore the catalytic hydrogen peroxide wet denitrification process using copper slag as a solid waste material. First, various smelting slags were screened to determine the potential of copper slag to catalyze hydrogen peroxide. Then, the catalytic activity of copper slag phases at different stages of the copper smelting

process was evaluated. A multifactorial assessment of slow-cooled copper slag catalysts for denitrification was also carried out. By identifying the iron phases in the copper slag as the main source of catalytic activity sites, the key factors influencing the denitrification process were understood. The detection of reactive oxygen species and the determination of NO transformation products, formation pathways, and reaction mechanisms in the liquid phase further enhanced the understanding of this innovative denitrification process. The findings of this study are expected to provide valuable insights into the utilization of solid waste and the management of atmospheric flue gas in the non-ferrous industry, opening up new possibilities for sustainable environmental protection.

2. Materials and Methods

2.1. Materials

The slag samples were obtained from metal smelting facilities in Yantai and Jiangxi, China. According to the classification of slag, the types are lead–zinc slag (LZS), manganese slag (MS), and copper slag (CS), respectively. Due to the different process sections of copper smelting, they are classified as copper tailings (CS-T), bottom-blown furnace copper slag (CS-B), and slow-cooled copper slag (CS-S). Solid waste residue samples were pulverized to a particle size of 200 nm and collected for experimental backup. Detailed information on other chemicals is given in Appendix A. Unless otherwise stated, all chemicals and reagents are of analytical grade and do not require additional purification.

2.2. Characterization

Powder X-ray diffraction (XRD) measurements were carried out using a Rigaku Ultima IV diffractometer and Cu Kα radiation. X-ray photoelectron spectroscopy (XPS, Thermo Scientific K-Alpha, Thermo Fisher Scientific, Waltham, MA, USA) was used to measure the Fe valence state and the relative content of surface elements. The binding energy of all samples was corrected to the C 1s line at 284.8 eV. The elemental content of the solid waste slag samples was determined by X-ray fluorescence spectroscopy (XRF, EDX-8000 (Zetium), Malvern Panalytical, Almelo, The Netherlands). The NO_3^- and NO_2^- anions produced during the reaction were analyzed by ion chromatography (IC, 930 compact ic flex, Metrohm, Herisau, Switzerland). Electron paramagnetic resonance (EPR) spectra were obtained by a Bruker EMX micro spectrometer (EMX micro, Bruker, Billerica, MA, USA).

2.3. Experimental Methods

2.3.1. Experimental System

A schematic diagram of the experimental setup is shown in Figure 1. These devices can be categorized by configured gas, catalytic oxidation, and exhaust gas detection. The ideal concentrations and flow rates of NO, O_2, and N_2 in the simulated flue gas (40 Liter Cylinder, Dalian Specialty Gases Co., Ltd., Dalian, China) were regulated by a mass flow controller (D08-1F, Beijing Seven Star Electronics Co., Ltd., Beijing, China). The desired concentrations of NO and O_2 in the modeled flue gas were 200 ppmv and 10 vol%, respectively. The oxidative absorption of NOx from the crude slurry was carried out in a three-necked flask, which was heated and stirred in a thermostat oil bath (DF-101S, INESA Scientific Instruments Co., Ltd., Shanghai, China). The flue gas concentrations after liquid-phase catalytic oxidation and uptake were analyzed by a flue gas analyzer (ECOM J2KN, ECOM, Hamburg, Germany). Water vapor in the exit gas was removed with anhydrous calcium chloride through a drying tube before entering the flue gas analyzer and then into an exhaust gas cleaning unit containing 4 wt% $KMnO_4$ solution. The experimental conditions were: NOx concentration = 200 ppmv; O_2 concentration = 10 vol%; gas flow rate = 200

mL/min; Fe concentration in the catalyst = 1 g/L; H_2O_2 concentration = 1.0 mol/L; initial pH = 9.0; reaction temperature = 45 °C; and the total solution volume = 200 mL.

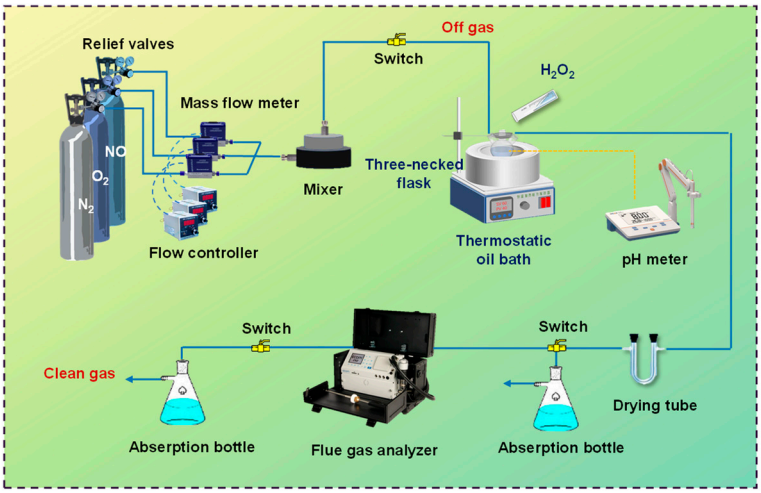

Figure 1. The NOx purification test system for catalytic oxidation.

2.3.2. Data Process

The NOx removal efficiency (η) and absorption capacity ($q_{ac,NO}$) of the experimental system were calculated as follows:

$$\eta(\%) = \frac{C_{inlet} - C_{outlet}}{C_{inlet}} \times 100\%$$

NOx absorption capacity (q_{ac}: absorption capacity)

$$q_{ac,NO}\left(mg(NO)\cdot L^{-1}\right) = \frac{Q\int_0^t (C_{inlet} - C_{outlet})dt}{1000\ V} \times \frac{30}{22.4}$$

where C_{inlet} and C_{outlet} denote the NOx concentration at the inlet flue gas and outlet flue gas of the catalytic oxidation system (ppmv). $q_{ac,NO}$ refers to the NOx absorption capacity (mg(NO) L^{-1}). Q, t, and V indicate the total gas flow rate (mL min^{-1}), the integration time (min), and the solution volume (L), respectively.

3. Results

3.1. Effect of Solid Waste Residues on NOx Removal

3.1.1. Effects of Different Types of Slag Slurry With and Without H_2O_2 on NOx Removal

Solid waste has a complex composition and is difficult to utilize in a high-value way [25]. To achieve sustainable green development in the industry, the residual value of transition metal-catalyzed hydrogen peroxide denitrification in solid waste was initially explored. We collected three different types of smelting slags from non-ferrous metal smelters, including copper slag (CS), manganese slag (MS), and lead–zinc slag (ZLS), which are typical iron, slam, and zinc-based waste slags, respectively. We first used XRD and XRF characterization techniques to determine the main chemical mineral phase composition of the slag. The main components of raw MS are $Ca_3Mg(SiO_4)_2$, $Ca_{0.96}Mn_{0.32}Si_{0.64}O_{2.56}$, and MnS, as shown in Figure 2a. According to XRF analyses, the main elements in these manganese slags are manganese, silicon, and calcium, and they are essentially free of iron (Table A1). The de-NOx efficiency in the MS/H_2O_2 system decreased rapidly to 16.1% at the beginning of 68.5%. This may be due to the presence of a large number of reducing phases and manganese ions leaching from the MS, which consume part of the oxidant by reacting with the oxidant and excessively decomposing H_2O_2 into O_2 (Equation (1)),

leading to a decrease in denitrification efficiency. In addition, the main components in raw LZS include $CaMnSi_2O_6$, $ZnSiO_3$, SiO_2, and ZnO [26]. The de-NOx efficiency in the ZC/H_2O_2 system is superior to the MS/H_2O_2 system. It is worth noting that the raw LZC fraction contains a large number of iron oxides, including FeO, Fe_3O_4, and Fe_2SiO_4 (Figure 2a and Table A1) [19,26]. It has been reported that H_2O_2 could be catalyzed by iron oxides to generate free radicals for the removal of NOx. The main minerals in raw CS are Fe_3O_4 and Fe_2SiO_4, with minor SiO_2 [15,22,27]. It was found that the maximum removal of NOx in the CS/H_2O_2 system was ~71.8% with a denitrification capacity of up to 27.8×10^{-2} mmol (Figure 2b,c), which was higher than the former two groups (MS/H_2O_2 and LZS/H_2O_2). Based on the analysis of XRF in Table A1, the content of Fe_2O_3 in raw CS (57.56%) was higher than that of raw LZC (42.16%) and raw MS (0%). This coincides with the phenomenon that higher iron levels favor denitrification. Furthermore, the effectiveness of transition metal-catalyzed hydrogen peroxide in solid wastes was demonstrated by the fact that denitrification with hydrogen peroxide alone was only 55.2% effective within 15 min. The de-NOx efficiencies of the three different types of smelter slurry without H_2O_2 were about ~10%~15%, suggesting that the use of smelter slag as an absorbent lone is virtually useless for denitrification.

$$2H_2O_2 + Mn^{4+}/Mn^{2+} \rightarrow 2H_2O + O_2 + Mn^{4+}/Mn^{2+}, \quad (1)$$

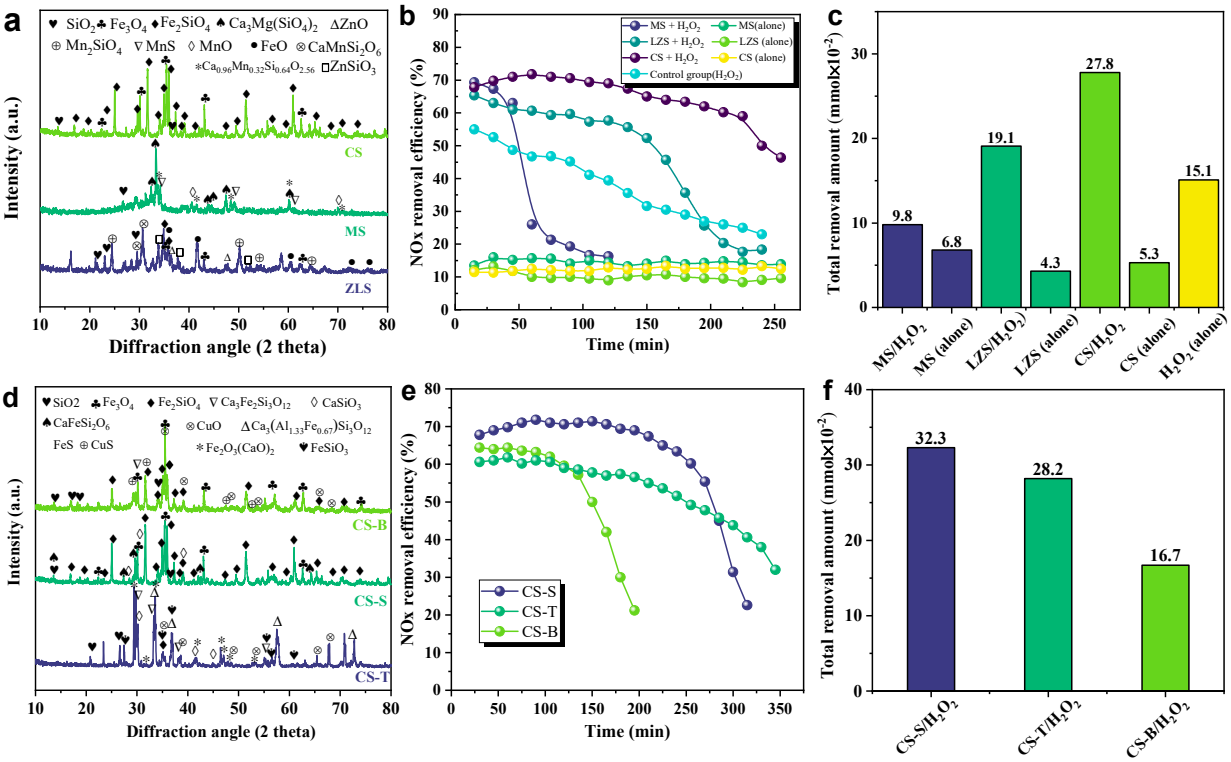

Figure 2. (**a**) XRD (**b**) denitrification efficiency and (**c**) denitrification capacity for different slags (in 250 min); and (**d**) XRD (**e**) denitrification efficiency and (**f**) denitrification capacity for different copper slags (in 300 min).

3.1.2. Effects of Different Types of H_2O_2/Copper Slag Slurry on NOx Removal

As shown in Table A2, copper slag is rich in the iron phase and may perform better when the iron is used as a catalyst to catalyze hydrogen peroxide denitrification [28]. However, different sections of the copper smelting process produce copper slag with varying proportions of iron, copper, and silicon as the copper element continues to be

refined. The copper tailings (CS-T) at the front end of the process have a high proportion of copper (7.06%), while the bottom-blown copper slag (CS-B) and slow-cooled copper slag (CS-S) at the back end of the process have relatively high contents of iron (51.75% and 57.56%). In order to investigate the denitrification potential of solid wastes generated from different copper smelting process segments, copper tailings, bottom-blown copper slag, and slow-cooled copper slag collected from various production stages of the copper smelting process were utilized for the assessment of denitrification activity. As shown in Figure 2d, XRD indicates that the main minerals in the original CS-B/S are Fe_3O_4 and Fe_2SiO_4, with a small amount of SiO_2 [22]. In comparison, the main components of CS-T are $Ca_3Fe_2Si_3O_{12}$ and CuO. As illustrated in Figure 2e,f, the de-NOx efficiency of 72.5% for the CS-S/H_2O_2 system was superior to the CS-S/H_2O_2 (64.3%) or CS-T/H_2O_2 (61.6%). The CS-S/H_2O_2 system has the highest denitrification capacity, so the slow-cooled copper slag is a potential material for catalytic hydrogen peroxide removal of NO in the copper smelting process section.

In order to explore the influence of individual key components in the copper slag, we also conducted control experiments with pure substances. As shown in Figure S1, the denitrification efficiency of the pure substance of Fe_3O_4 is as high as 80.5%, which is ~10% higher than the control of CS-S. The octahedral site of the magnetite spinel structure is a very flexible redox site that can accommodate both Fe^{3+} and Fe^{2+} [29], which suggests that the effect of Fe_3O_4 on NOx removal is relatively high in the CS-S/H_2O_2 system [30,31]. In the system of CS-T/H_2O_2, CuO leads to faster consumption and lower utilization of H_2O_2 under alkaline conditions [22], which leads to a decrease in denitrification efficiency from 70.2% to 15.9% after 120 min (Figure 2e), which is consistent with the trend of the pure substance control experiment (Figure S1). The denitrification effect was not significant for other material phases that may be present in the copper slag, such as SiO_2 and FeO. The CS-T seems to be unfavorable for providing effective active sites for activated H_2O_2 due to the highly crystalline coexisting mineral phase, including $Ca_3Fe_2Si_3O_{12}$, $Ca_3Al_{1.33}Fe_{0.67}Si_3O_{12}$, and $Fe_2O_3(CaO)_2$. Hence, slow-cooled copper slag was chosen as a material for an in-depth study of the mechanism in this research.

3.2. Optimization of Denitrification Performance

In order to optimize the ideal operating conditions of the CS-S/H_2O_2 system, the effects of pH, H_2O_2 concentration, temperature, and slag dose on denitrification were investigated [30,32,33]. To avoid the mutual interference of several factors, we controlled the variables of the effects of single-factor denitrification experiments in our study.

As illustrated in Figure 3a, the pH value has a significant influence on the formation of free radicals and NOx adsorption. The effects of the initial pH value on NOx removal efficiency at 3.0–11.0 were investigated. When the starting pH of the solution was increased from 3.0 to 9.0, the maximum removal of NOx increased from approximately 32.9% to nearly 73.3%. There will be more chance to react with NOx before the $O_2^{\bullet -}$ extinguishment, increasing the removal rate of NOx [34]. In addition, the pH value may affect the generation of the type of reactive oxygen species in the system, which in turn affects the affinity for NOx binding. The pH increased to between 9.0 and 11.0, and the denitrification efficiency began to decrease. This suggests that the following side reactions (Equations (2)–(4)) may be occurring in the system, reducing the amount of active species [22].

The oxidizing capacity of the system is highly dependent on the concentration of H_2O_2, which in turn affects the generation of free radicals and the ability to remove NOx (Figure 3b). An optimal de-NOx performance was obtained at 1.0 M H_2O_2. Further increasing or decreasing the H_2O_2 concentration causes a decreased NOx removal ability due to

radical scavenging effect at high H_2O_2 concentrations or insufficient radical generation at low H_2O_2 concentrations [32,33].

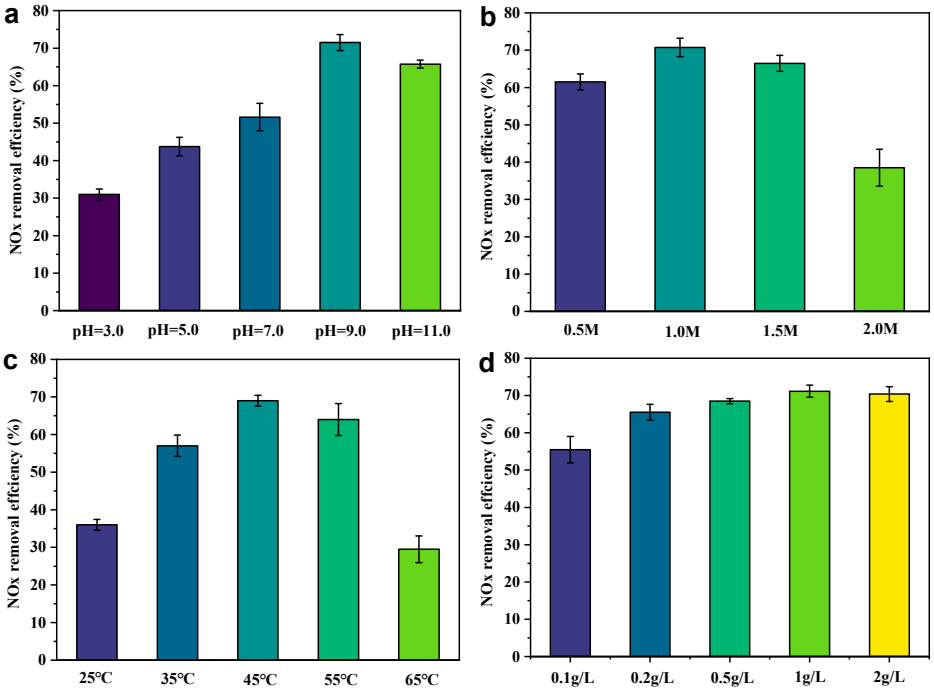

Figure 3. Effect of (**a**) pH, (**b**) H_2O_2 concentration, (**c**) temperature, and (**d**) slag dose on NOx removal. Experimental conditions: NOx concentration = 200 ppmv; O_2 concentration = 10 vol%; gas flow rate = 200 mL/min; dosage of waste residue = 1 g/L; H_2O_2 concentration = 1.0 mol/L; initial pH = 9.0; reaction temperature = 45 °C; and total solution volume = 200 mL.

As shown in Figure 3c, the denitrification efficiency is only 35.1% when the liquid phase temperature is at 25 °C. When the temperature continues to increase to 45 °C, the denitrification efficiency rises by 42.8% to 72.7%. According to the Arrhenius formula (lnK~1/T) [35], raising the reaction temperature leads to an exponential increase in the value of the reaction kinetics of the system in solution. This promotes collisional contact between NO and reactive oxygen species in the liquid phase and improves denitrification efficiency. However, high temperatures (45 °C to 65 °C) can also lead to the premature depletion of hydrogen peroxide, which plummets denitrification efficiency.

Also, the CS-S catalyst exhibits a dosage-dependent NOx removal activity (Figure 3d). The NOx removal efficiency increased with the increase in catalyst dosage, and it obtained its maximum NOx removal amount at a catalyst concentration of 1 g L^{-1}.

$$H_2O_2 \leftrightarrow HO_2^- + H^+, \quad (2)$$

$$OH + HO_2^- \rightarrow OH^- + HO_2, \quad (3)$$

$$H_2O_2 + HO_2^- \rightarrow H_2O + O_2 + OH^-, \quad (4)$$

3.3. Liquid Phase System Analysis of Slurry with H_2O_2/CS-S

3.3.1. Reactive Oxygen Species (ROS) in H_2O_2/CS-S

To understand the formation pathway of free radicals via H_2O_2 activation in the CS-S/H_2O_2 system, we first performed chemical quenching experiments with different scavengers to further identify the major ROS. We selected methanol (MeOH), p-benzoquinone (p-BQ), and furfuryl alcohol (FFA) as the quenching agents for the ·OH, $\cdot O_2^-$, and $^1O_2$ radicals, respectively [36]. The quenching experiments in Figure 4a show that denitrifica-

tion efficiency was mildly suppressed in the absence of MeOH and FFA, decreasing from ~72% to ~68% and ~64%, respectively, at 60 min. In contrast, p-BQ significantly inhibits NOx removal, resulting in a decrease in NOx removal of approximately 24% at 60 min. Combining the results of MeOH/TBA and p-BQ, it is clear that $\cdot O_2^-$ plays a dominant role in NOx oxidation [37]. In addition, MeOH/FFA also inhibited the NOx removal efficiency (by about ~4%~8%), indicating that ·OH and $^1O_2$ radicals are not the key reactive oxygen species for NO oxidation. The inhibitory effect of p-BQ suggests that the formation pathway of $\cdot O_2^-$, a key oxygen species of free radicals, is closely related to the chain reaction in the iron phase (Fe^{2+}/Fe^{3+}) on the slow-cooled slag surface.

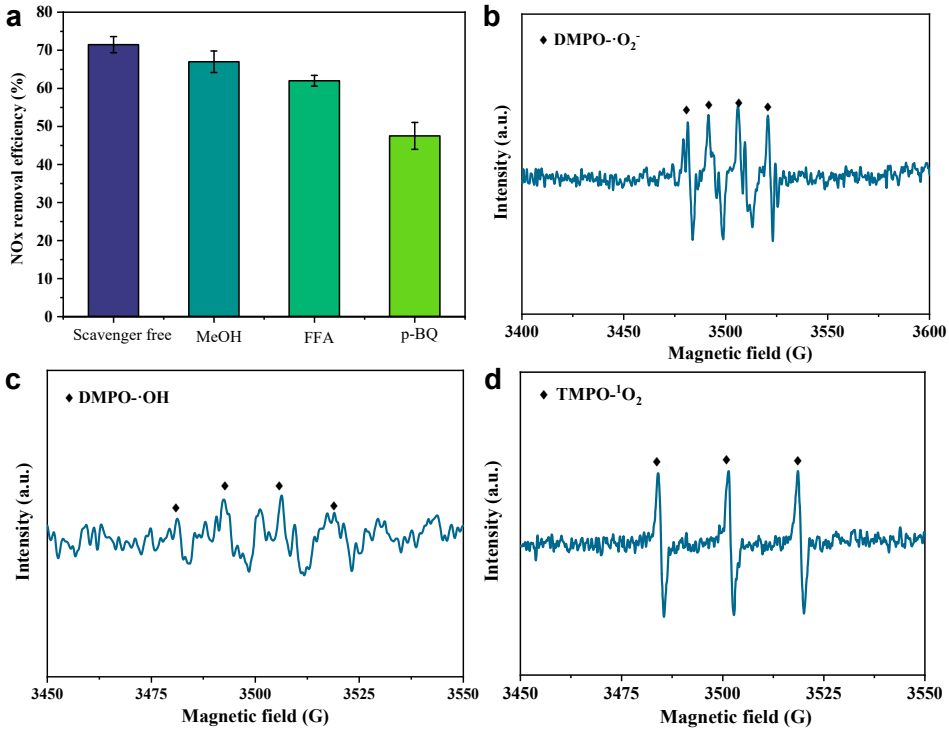

Figure 4. (**a**) Effect of different scavengers on NOx and removing efficiency (at 60 min) in the CS-S/H_2O_2 system; DMPO spin-trapping EPR spectra in (**b**) methanol and (**c**) water system; (**d**) TMPO spin-trapped EPR spectra in the aqueous regime.

We further characterized the radical formation by EPR experiments using 5,5-dimethyl-1-pyrroline N-oxide (DMPO) as a spin-trapping agent [36]. As shown in Figure 4b, in the methanol system, the trapping agent DMPO captured four 1:1:1:1 (CS-S-DMPO-·O_2^-) characteristic peaks, which were defined as superoxide radicals. This is strong evidence indicating that superoxide radicals are the major reactive oxygen species in the liquid phase system. In addition, as shown in Figure 4c,d, we also detected characteristic peaks with intensities of 1:2:2:1 and 1:1:1 (CS-S-DMPO-·OH and CS-S-TMPO-$^1O_2$), which were attributed to ·OH and $^1O_2$, consistent with the results of the bursting experiments. This further suggests that the affinity of different slags to catalyze hydrogen peroxide into different radical species directly affects the NOx and removal efficiency.

3.3.2. Analysis of Denitrification Products

Meanwhile, to reveal the reaction mechanism pathway for the removal of NO pollutants by the CS-S/H_2O_2 system, the variation in the liquid products was also observed and followed by IC measurements. As shown in Figure 5a, the major products of NO production in the CS-S/H_2O_2 reaction system are high-valent nitrate and nitrite (NO_2^- and NO_3^-) [25]. NO_3^- was the dominant denitrification product in the first 120 min

compared to NO_2^- [7]. In addition, the ratio of NO_2^- to NO_3^- was approximately ~1:1 after 240 min, as shown in Figure 5b. Therefore, the following chain reaction pathway exists in the reaction mechanism for NO removal (Equations (5)–(10)) [7,22,30].

$$NO + O_2^{\bullet -} \rightarrow NO_3^-, \quad (5)$$

$$NO + O_2^{\bullet -} \rightarrow NO_2^- + O^-, \quad (6)$$

$$NO_2 + O^- \rightarrow NO_3^-, \quad (7)$$

$$NO + \bullet OH \rightarrow H^+ + NO_2^-, \quad (8)$$

$$NO_2 + \bullet OH \rightarrow H^+ + NO_3^-, \quad (9)$$

$$^1O_2 + NO \rightarrow NO_2, \quad (10)$$

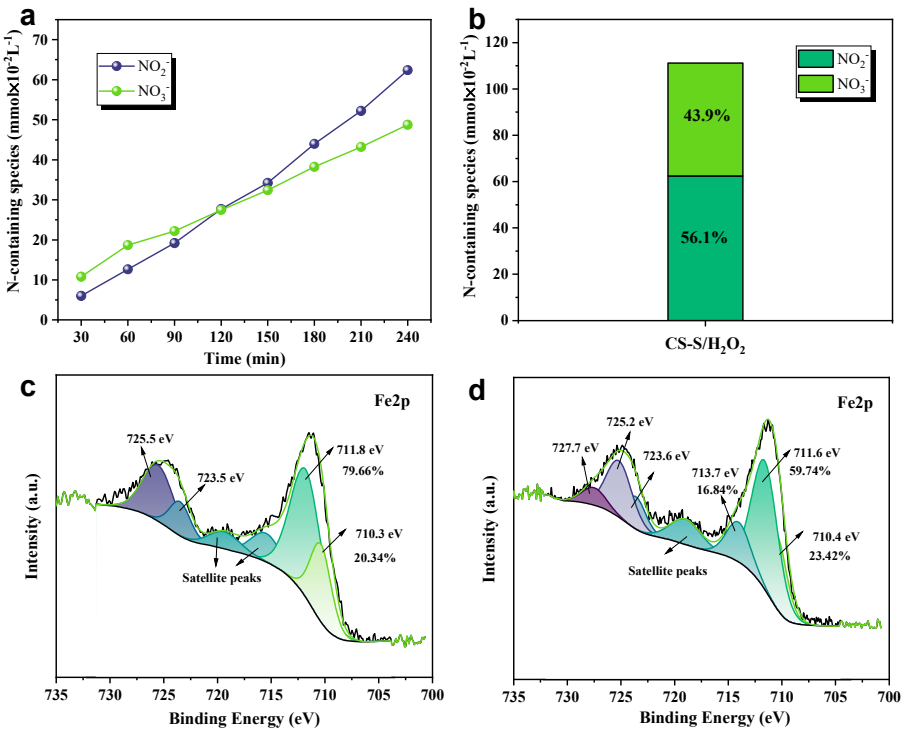

Figure 5. (**a**) Change in ionic concentration of reaction products. (**b**) Distribution of N-containing liquid species after 240 min of reaction. X-ray photoelectron spectroscopy (XPS) patterns of Fe 2p from (**c**) fresh and (**d**) spent copper slag.

3.3.3. Surface of CS-S Before and After Liquid-Phase Reaction

To explore the mechanism of catalytic hydrogen peroxide denitrification by copper slag waste and to observe the valence changes on the surface of the material, we will perform XPS on the material before and after the described reaction. The Fe 2p spectra of fresh and used slow-cooled copper slag are shown in Figure 5c. The B.Es located at approximately 709.8–710.4 eV for Fe $2p_{3/2}$ and 723.3–723.7 eV for Fe $2p_{1/2}$ indicate the presence of Fe(II), while the peaks at 711.4-711.9 eV for Fe $2p_{3/2}$ and the peak at 725.2–725.5 eV for Fe $2p_{1/2}$ are indicative of the presence of Fe(III) [30,33]. Before the reaction, the main Fe^{2+} and Fe^{3+} valence iron contents of the Fe phase were 20.34% and 79.66%, respectively. After the response, the Fe $2p_{3/2}$ peak at 713.1 eV indicates the presence of Fe^{3+}-OH, which may be obtained from the surface hydroxyl groups generated by the liquid phase after the reaction [30]. After the CS-S reaction, the Fe^{2+}/Fe^{3+} ratio decreased from 3.92 to 3.70, indicating that the percentage of Fe^{2+} and Fe^{3+} content on the surface

of CS-S in the system changed dynamically. This phenomenon change may be related to the experimental mechanism of reactive oxygen species generation, and the related chemical equations (Equations (11) and (12)) [7,22,38,39] are as follows. Finally, in order to further explain this issue, we also supplemented this material with replicated experiments (e.g., Figure S2), which showed that the denitrification performance of this material is very reproducible and can further side-step the possible existence of the Fe^{2+}/Fe^{3+} cycle [40].

$$Fe^{2+} + H_2O_2 \rightarrow Fe^{3+} + \bullet OH + OH^-, \quad (11)$$

$$Fe^{3+} + H_2O_2 \rightarrow Fe^{2+} + O_2^{\bullet -} + 2H^+, \quad (12)$$

4. Discussion

Based on the aforementioned experimental results, as depicted in Figure 6, a plausible mechanism for the wet denitrification of nitrifying tail gas through the use of copper slag-catalyzed hydrogen peroxide was put forward. In slow-cooled copper slag, the primary components are iron olivine and magnetite. In the H_2O_2/copper slag system, the iron phases within the slow-cooled copper slag play a pivotal role. The Fe^{2+}/Fe^{3+} sites on the surface of the iron phase are capable of activating H_2O_2 via a series of reactions. Initially, H_2O_2 can react with Fe^{2+} to generate ·OH radicals and Fe^{3+} (as shown in Equation (11)). Subsequently, Fe^{3+} can be reduced back to Fe^{2+} when it reacts with another H_2O_2 molecule concurrently generating $\cdot O_2^-$ radicals (as per Equation (12)).

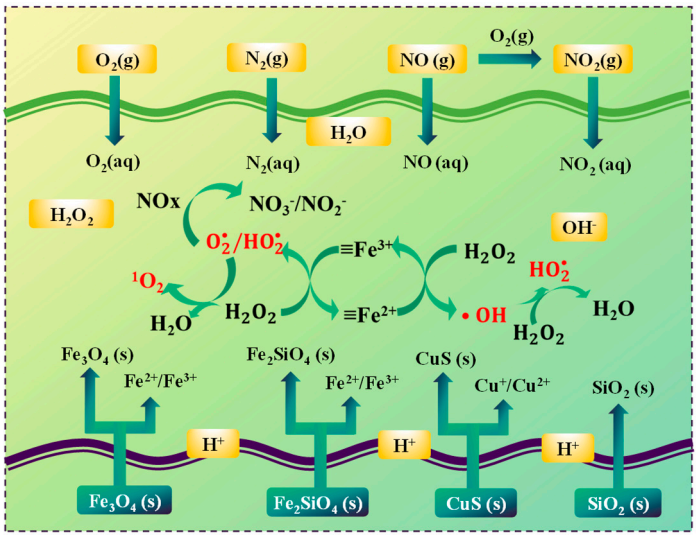

Figure 6. Reaction mechanism of removal of NOx by H_2O_2/slow-cooled copper slag slurry.

As ascertained by the reactive oxygen species (ROS) analysis,$\cdot O_2^-$ emerges as the dominant reactive oxygen species responsible for the oxidation of NOx. NO can react with $\cdot O_2^-$ to form NO_2^- and NO_3^- (as described in Equations (6) and (5)). Additionally, ·OH and $^1O_2$ also partake in the reaction to a certain degree, oxidizing NO to higher-valence nitrogen oxides (as indicated by Equations (8)–(10)).

The reaction conditions, such as pH, H_2O_2 concentration, temperature, and slag dosage, can exert a profound influence on the generation and activity of reactive oxygen species, thereby affecting the denitrification efficiency. For example, the pH value has an impact on the dissociation of H_2O_2 and the formation of diverse reactive oxygen species. An optimal pH can facilitate the reaction between NOx and reactive oxygen species. The H_2O_2 concentration directly determines the quantity of reactive oxygen species produced. Excessively high concentrations of H_2O_2 may lead to radical scavenging, whereas low concentrations result in inadequate radical generation. Temperature affects the reaction

kinetics. An increase in temperature can enhance the collision frequency between NO and reactive oxygen species, but an overly high temperature will cause premature depletion of H_2O_2. The slag dosage affects the number of active sites available for the activation of H_2O_2, which in turn influences the overall denitrification process.

5. Conclusions

This study explored the catalytic hydrogen peroxide wet denitrification process using copper slag, aiming to address environmental issues in the non-ferrous metal industry. Through screening different smelting slags, copper slag was found to have great catalytic potential for hydrogen peroxide in NOx removal. Among various copper slags, slow-cooled copper slag (CS-S) showed the best performance, mainly due to Fe_3O_4 in its structure. The optimization results indicated that the optimal conditions for the H_2O_2/CS-S system were an initial pH of 9.0, a H_2O_2 concentration of 1.0 M, a temperature of 45 °C, and a slag dose of 1 g/L. Analysis of the liquid phase system revealed that $\cdot O_2^-$ was the dominant reactive oxygen species for NOx oxidation. The main denitrification products were nitrate and nitrite. XPS analysis showed valence changes in Fe on the copper slag surface. Overall, this research provides an eco-friendly method for copper slag utilization and NOx control in the non-ferrous metal industry, offering new prospects for sustainable industrial development. Future research can focus on scaling up the process and improving its industrial applicability.

Supplementary Materials: The following supporting information can be downloaded at: https://www.mdpi.com/article/10.3390/su17062469/s1, Figure S1: Simulation of denitrification experiments with a single pure substance in Copper slag (CS-S); Figure S2: Experiments on denitrification cycle using copper slag (CS-S).

Author Contributions: Conceptualization, methodology and validation, H.T.; formal analysis, J.B.; investigation, C.L.; resources, Y.D.; data curation and writing—original draft preparation, H.T.; writing—review and editing and visualization, S.B. and X.S.; supervision and project administration, Y.M. and L.S.; funding acquisition, K.L. and P.N. All authors have read and agreed to the published version of the manuscript.

Funding: This work was supported by the National Natural Science Foundation of China [52270106, 22266021], Yunnan Major Scientific and Technological Projects (grant NO. 202202AG050005), and Yunnan Key Laboratory of Phosphogypsum Recycling and Ecological Utilization (202449CE340028).

Institutional Review Board Statement: Not applicable.

Informed Consent Statement: Not applicable.

Data Availability Statement: The authors confirm that data supporting the study's findings are provided in the article.

Conflicts of Interest: The authors declare no competing financial interests or personal relationships that could have influenced the work reported in this paper.

Appendix A

Chemicals

Unless otherwise specified, all chemicals and reagents were of analytical grade (AR) and used without further purification. Methanol (CH_3OH, 99.5%) and Furfuryl alcohol (FFA, 99.0%) were purchased from Macklin (Shanghai, China). Hydrogen peroxide (H_2O_2, 30 wt%), p-Benzoquinone (p-BQ, ≥99.0%), 5,5-Dimethyl-1-pyrroline N-oxide (DMPO, ≥97%), 2,2,6,6-Tetramethylpiperidine (TEMP, ≥98.0%) were purchased from Aladdin (Shanghai, China).

Table A1. Determination of the main chemistry of different types of smelting slag by XRF.

Sample	Fe_2O_3 *	SiO_2 *	SO_3 *	CaO *	CuO *	Al_2O_3 *	ZnO *	MnO *
ZLS	42.16	21.36	-	10.86	-	-	6.30	13.50
MS	-	28.13	5.27	41.02	-	6.90	-	16.34
CS	57.56	31.85	0.76	4.22	0.30	-	3.38	0.26

* Content of elements in the form of oxides and other components with a content of less than 1% are not listed.

Table A2. Determination of the main chemistry of different types of copper slag by XRF.

Sample	Fe_2O_3 *	SiO_2 *	SO_3 *	CaO *	CuO *	Al_2O_3 *	ZnO *	MnO *	P_2O_5 *
CS-T	17.25	30.31	1.65	31.61	7.06	4.80	0.10	1.00	5.50
CS-S	57.56	31.85	0.76	4.22	0.30	-	3.38	0.26	-
CS-B	51.75	23.81	9.67	2.33	6.34	-	3.27	0.17	-

* Content of elements in the form of oxides and other components with a content of less than 1% are not listed.

References

1. Hong, J.G.S.; Abdullah, N.; Rajaratnam, R.K.; Shukri, S.A.; Tan, S.P.; Hamdan, M.; Lim, B.K. Combined perineal massage and warm compress compared to massage alone during active second stage of labour in nulliparas: A randomised trial. *Eur. J. Obstet. Gynecol. Reprod. Biol.* **2022**, *270*, 144–150. [CrossRef] [PubMed]
2. Cao, Y.; Ma, Q.; Chu, B.; He, H. Homogeneous and heterogeneous photolysis of nitrate in the atmosphere: State of the science, current research needs, and future prospects. *Front. Environ. Sci. Eng.* **2023**, *17*, 48. [CrossRef]
3. Ding, X.H.; Luo, B.; Zhou, H.T.; Chen, Y.H. Generalized solutions for advection–dispersion transport equations subject to time- and space-dependent internal and boundary sources. *Comput. Geotech.* **2025**, *178*, 106944. [CrossRef]
4. Elkaee, S.; Phule, A.D.; Yang, J.H. Advancements in (SCR) technologizes for NOx reduction: A comprehensive review of reducing agents. *Process Saf. Environ. Prot.* **2024**, *184*, 854–880. [CrossRef]
5. Zhao, M.; Xue, P.; Liu, J.; Liao, J.; Guo, J. A review of removing SO_2 and NOx by wet scrubbing. *Sustain. Energy Technol. Assess.* **2021**, *47*, 101451. [CrossRef]
6. Yuan, B.; Mao, X.; Wang, Z.; Hao, R.; Zhao, Y. Radical-induced oxidation removal of multi-air-pollutant: A critical review. *J. Hazard. Mater.* **2020**, *383*, 121162.1–121162.13. [CrossRef]
7. Wang, X.; Bao, J.; Zi, S.; Luo, Y.; Liu, C.; Zeng, Z.; Wang, F.; Yang, J.; Shi, L.; Li, K.; et al. Insight into NOx removal mechanism by H_2O_2 activation via MIL-100(Fe) in an alkaline environment. *J. Environ. Chem. Eng.* **2024**, *12*, 113456. [CrossRef]
8. Song, L.; Deng, S.; Bian, C.; Liu, C.; Zhan, Z.; Li, S.; Li, J.; Fan, X.; He, H. NiB_2O_4 (B = Mn or Co) catalysts for NH_3-SCR of NOx at low-temperature in microwave field. *Front. Environ. Sci. Eng.* **2023**, *17*, 96. [CrossRef]
9. Choi, S.W.; Choi, S.K.; Bae, H.K. Hybrid selective noncatalytic reduction (SNCR)/selective catalytic reduction (SCR) for NOx removal using low-temperature SCR with Mn-V_2O_5/TiO_2 catalyst. *J. Air Waste Manag. Assoc.* **2015**, *65*, 485–491. [CrossRef]
10. Zhou, X.; Chen, X.; Peng, Z.; Zhou, Y.; Li, Y.; Jian, W.; Fan, Z.; Chen, Y. Cleaner geopolymer prepared by co-activation of gasification coal fly ash and steel slag: Durability properties and economic assessment. *Front. Environ. Sci. Eng.* **2023**, *17*, 109–121. [CrossRef]
11. Cheng, S.; Li, W.; Han, Y.X.; Sun, Y.S.; Gao, P.; Zhang, X. Recent process developments in beneficiation and metallurgy of rare earths: A review. *J. Rare Earths* **2023**, *42*, 629–642. [CrossRef]
12. Deng, S.; An, Q.; Ran, B.; Yang, Z.; Xu, B.; Zhao, B.; Li, Z. Efficient remediation of Mn^{2+} and NH_4^+-N in co-contaminated water and soil by *Acinetobacter* sp. AL-6 synergized with grapefruit peel biochar: Performance and mechanism. *Water Res.* **2022**, *223*, 118962. [CrossRef] [PubMed]
13. Meng, Z.; Wang, C.; Wang, X.; Chen, Y.; Wu, W.; Li, H. Simultaneous removal of SO_2 and NOx from flue gas using $(NH_4)_2S_2O_3$/steel slag slurry combined with ozone oxidation. *Fuel* **2019**, *255*, 115760.1–115760.8. [CrossRef]
14. Zhao, H.X.; Zhou, F.S.; LM, A.E.; Liu, J.L.; Zhou, Y. A review on the industrial solid waste application in pelletizing additives: Composition, mechanism and process characteristics. *J. Hazard. Mater.* **2021**, *423*, 127056. [CrossRef]
15. Bao, J.; Ning, P.; Wang, F.; Sun, X.; Wang, C.; Song, X.; Luo, Y.; Li, K. Thermal modification of copper slag via phase transformation for simultaneous removal of SO_2 and NOx from acid-making tail gas. *Chem. Eng. J.* **2021**, *425*, 131646. [CrossRef]
16. Tang, Y.; Wei, Z.; Wang, C.; Ning, P.; He, M.; Bao, S.; Sun, X.; Li, K. One-step synthesis of magnetic catalysts containing Mn_3O_4-Fe_3O_4 from manganese slag for degradation of enrofloxacin by activation of peroxymonosulfate. *Chem. Eng. J.* **2024**, *499*, 156505. [CrossRef]

17. OuYang, K.; Dou, Z.H.; Zhang, T.A.; Liu, Y.; Niu, L.P. Desulfurization kinetics of high lead and zinc sulfide containing slag with oxygen blowing. *J. Min. Metall. Sect. B Metall.* **2019**, *55*, 26. [CrossRef]
18. Su, Y.; Luo, B.; Luo, Z.; Xu, F.; Huang, H.; Long, Z.; Shen, C. Mechanical characteristics and solidification mechanism of slag/fly ash-based geopolymer and cement solidified organic clay: A comparative study. *J. Build. Eng.* **2023**, *71*, 106459. [CrossRef]
19. Radulović, D.; Terzić, A.; Stojanović, J.; Jovanović, V.; Todorović, D.; Ivošević, B. Reapplication Potential of Historic Pb–Zn Slag with Regard to Zero Waste Principles. *Sustainability* **2024**, *16*, 720. [CrossRef]
20. Arredondo, P.W.C.; Silva, Y.F.; Araya-Letelier, G.; Hernández, H. Valorization of Recycled Aggregate and Copper Slag for Sustainable Concrete Mixtures: Mechanical, Physical, and Environmental Performance. *Sustainability* **2024**, *16*, 11239. [CrossRef]
21. Li, J.; Eheliyagoda, D.; Geng, Y.; Yang, Z.; Zeng, X. Examining the influence of copper recycling on prospective resource supply and carbon emission reduction. *Fundam. Res.* **2022**, *9*, 022. [CrossRef]
22. Bao, J.; Yang, J.; Song, X.; Han, R.; Ning, P.; Lu, X.; Fan, M.; Wang, C.; Sun, X.; Li, K. The mineral phase reconstruction of copper slag as Fenton-like catalysts for catalytic oxidation of NOx and SO_2: Variation in active site and radical formation pathway. *Chem. Eng. J.* **2022**, *450*, 138101. [CrossRef]
23. Wang, H.; Yuan, B.; Hao, R.; Zhao, Y.; Wang, X. A critical review on the method of simultaneous removal of multi-air-pollutant in flue gas. *Chem. Eng. J.* **2019**, *378*, 122155. [CrossRef]
24. Li, Y.; Zhu, X.; Qi, X.; Shu, B.; Zhang, X.; Li, K.; Wei, Y.; Wang, H. Removal and immobilization of arsenic from copper smelting wastewater using copper slag by in situ encapsulation with silica gel. *Chem. Eng. J.* **2020**, *394*, 124833. [CrossRef]
25. Liu, X.; Li, S.; Ren, Z.; Cao, H.; Yang, Q.; Luo, Z.; He, L.; Zhao, J.; Wang, Q.; Li, G. Hydrogen Peroxide Heterolytic Cleavage Induced Gas Phase Photo-Fenton Oxidation of Nitric Oxide. *Environ. Sci. Technol.* **2024**, *58*, 17797–17806. [CrossRef]
26. Luo, S.; Zhao, S.; Zhang, P.; Li, J.; Huang, X.; Jiao, B.; Li, D. Co-disposal of MSWI fly ash and lead–zinc smelting slag through alkali-activation technology. *Constr. Build. Mater.* **2022**, *327*, 127006. [CrossRef]
27. Escobedo, E.; Oh, J.-A.; Cho, K.; Chang, Y.-S. Activation of hydrogen peroxide, persulfate, and free chlorine by steel anode for treatment of municipal and livestock wastewater: Unravelling the role of oxidants speciation. *Water Res.* **2022**, *216*, 118305. [CrossRef]
28. Atran, A.A.; Ibrahim, F.A.; Awwad, N.S.; Hamdy, M.S. Iron incorporated porous cerium oxide nanoparticles as an efficient photocatalyst for different hazardous elimination. *J. Rare Earths* **2024**, *02*, 006. [CrossRef]
29. Costa, R.C.C.; Moura, F.C.C.; Ardisson, J.D.; Fabris, J.D.; Lago, R.M. Highly active heterogeneous Fenton-like systems based on Fe^0/Fe_3O_4 composites prepared by controlled reduction of iron oxides. *Appl. Catal. B Environ.* **2008**, *83*, 131–139. [CrossRef]
30. Yang, B.; Ma, S.; Cui, R.; Sun, S.; Wang, J.; Li, S. Simultaneous removal of NOx and SO_2 with H_2O_2 catalyzed by alkali/magnetism-modified fly ash: High efficiency, Low cost and Catalytic mechanism. *Chem. Eng. J.* **2019**, *359*, 233–243. [CrossRef]
31. Yang, S.; Xu, D.; Yan, W.; Xiong, Y. Effective NO and SO_2 removal from fuel gas with H_2O_2 catalyzed by $Fe_3O_4/Fe^0/Fe_3C$ encapsulated in multi-walled carbon nanotubes. *J. Environ. Chem. Eng.* **2021**, *9*, 105413. [CrossRef]
32. Huang, T.; Zhang, G.; Zhang, N.; Ye, J.; Lu, P. Fe^0-H_2O_2 for advanced treatment of citric acid wastewater: Detailed study of catalyst after several times use. *Chem. Eng. J.* **2018**, *336*, 233–240. [CrossRef]
33. Wan, Z.; Wang, J. Degradation of sulfamethazine using Fe_3O_4-Mn_3O_4/reduced graphene oxide hybrid as Fenton-like catalyst. *J. Hazard. Mater.* **2017**, *324*, 653–664. [CrossRef]
34. Sun, B.; He, M.; Chi, H.; Wang, Z.; Zhang, W.; Ma, J. Highly efficient simultaneous catalytic degradation and defluorination of perfluorooctanoic acid by the H_2O_2-carbon/MnO_2 system generating $\cdot O_2^-$ and ·OH synchronously. *Appl. Catal. B Environ.* **2020**, *277*, 119219.
35. Sarkar, D.; Kang, P.; Nielsen, S.O.; Qin, Z. Non-Arrhenius Reaction-Diffusion Kinetics for Protein Inactivation over a Large Temperature Range. *ACS Nano* **2019**, *13*, 8669–8679. [CrossRef]
36. Wang, L.; Lan, X.; Peng, W.; Wang, Z. Uncertainty and misinterpretation over identification, quantification and transformation of reactive species generated in catalytic oxidation processes: A review. *J. Hazard. Mater.* **2021**, *408*, 124436. [CrossRef]
37. Watts, R.J.; Teel, A.L. Hydroxyl radical and non-hydroxyl radical pathways for trichloroethylene and perchloroethylene degradation in catalyzed H_2O_2 propagation systems. *Water Res.* **2019**, *159*, 46–54. [CrossRef]
38. Pham, L.T.; Lee, C.; Doyle, F.M.; Sedlak, D.L. A Silica-Supported Iron Oxide Catalyst Capable of Activating Hydrogen Peroxide at Neutral pH Values. *Environ. Sci. Technol.* **2009**, *43*, 8930–8935. [CrossRef]
39. Yang, W.; Chen, L.; Zhou, B.; Jia, Z.; Liu, X.; Liu, Y.; Li, H.; Gao, Z. NO Oxidation Using H_2O_2 at a Single-Atom Iron Catalyst. *J. Phys. Chem. C* **2023**, *127*, 13011–13020. [CrossRef]
40. Hu, K.; Zhou, P.; Yang, Y.; Zhong, S.; Duan, X.; Wang, S. The Nature of Molecular Hybridizations in Nanodiamonds for Boosted Fe(III)/Fe(II) Circulation. *Environ. Sci. Technol.* **2024**, *58*, 20665–20675. [CrossRef]

Disclaimer/Publisher's Note: The statements, opinions and data contained in all publications are solely those of the individual author(s) and contributor(s) and not of MDPI and/or the editor(s). MDPI and/or the editor(s) disclaim responsibility for any injury to people or property resulting from any ideas, methods, instructions or products referred to in the content.